

# Study of the Bipolar Nebula IRAS 19312+1950. II. Circumstellar Chemistry

Shuji DEGUCHI<sup>1,2</sup>, Jun-ichi NAKASHIMA<sup>2,3</sup>  
and

Shuro TAKANO<sup>1,2</sup>

<sup>1</sup> Nobeyama Radio Observatory, National Astronomical Observatory  
Minamimaki, Minamisaku, Nagano 384-1305

<sup>2</sup> Department of Astronomical Science, Graduate University for Advanced Studies,  
Nobeyama Radio Observatory, Minamimaki, Minamisaku, Nagano 384-1305

<sup>3</sup> Department of Astronomy, University of Illinois at Urbana/Champaign,  
1002 W Green St., Urbana, Illinois 61801, U. S. A.

(Received 2004 July 1; accepted 2004 September 29)

## Abstract

The bipolar nebula, IRAS 19312+1950, is a unique SiO maser source exhibiting both properties as young and evolved objects. To clarify the nature of this object, we made molecular line observations with the Nobeyama 45-m radio telescope. We detected emission from O-bearing ( $\text{HCO}^+$ , SiO, SO, and  $\text{SO}_2$ ), C- and N-bearing molecules (CN, CS, HCN, HNC,  $\text{NH}_3$ ,  $\text{N}_2\text{H}^+$ ,  $\text{HC}_3\text{N}$ ,  $\text{H}_2\text{CS}$ , and  $\text{CH}_3\text{OH}$ ), and their isotopic species ( $\text{C}^{17}\text{O}$ ,  $^{13}\text{C}^{18}\text{O}$ , and  $\text{C}^{34}\text{S}$ ). Line profiles consist of a weak broad ( $\Delta v \sim 30 \text{ km s}^{-1}$ ) and/or a strong narrow ( $\Delta v \lesssim 5 \text{ km s}^{-1}$ ) components, depending on molecular species. Strong time variations of  $\text{H}_2\text{O}$  and SiO masers were also observed. Numerical modeling of the envelope with the LVG-code results in a good fit of the model with a mass loss rate of  $2.6 \times 10^{-4} M_\odot \text{ yr}^{-1}$  to the observed intensities for the broad-component lines. On the other hand, non-O-bearing molecules, which have only the narrow profiles, were found to have abundances typical to those in cool dust clouds. No isotopic enrichment was found, indicating little evidence of the narrow cool component being an ejecta of the central AGB star or a possible companion. These facts compelled us to conclude that IRAS 19312+1950 is an exotic mass-losing evolved star embedded in a low-mass ( $\sim 20 M_\odot$ ) dark cloud.

**Key words:** stars: circumstellar matter, stars: individual (IRAS 19312+1950), stars: late-type

## 1. Introduction

IRAS 19312+1950 exhibits a prominent bipolar nebosity of the size of about  $30''$  in near-infrared images (Nakashima, Deguchi 2000). The IRAS color of this source,  $\log(F_{25}/F_{12}) = 0.47$ , indicates a presence of cool dust of a temperature of about 200 K toward this source. Detecting SiO and  $\text{H}_2\text{O}$  maser lines in this object, Nakashima, Deguchi (2000) concluded that this is an oxygen-rich protoplanetary nebula similar to OH231.8+4.2. The distance to this object was estimated to be about 2.5 kpc (Nakashima et al. 2004; hereafter Paper I), based on the near- and mid-IR flux densities. It is slightly unusual that CO and the other thermal molecular lines of less abundant species are detectable in the envelope of an Asymptotic Giant Branch (AGB) or post-AGB stars at 2.5 kpc away from the sun. For example, the distance to the similar object, OH231.8+4.2, is about 1.3 kpc (Morris et al. 1987), and those of other commonly observed AGB stars in radio are less than 1 kpc (Olofsson et al. 1998). Near-IR imaging of this object with the UH 88-inch telescope shows a bright central star and surrounding nebula, extending from NE to SW by about  $30''$  (figure 1). It also shows a small ( $\sim 5''$ ) ring-like structure near the central star, which is elongated perpendicularly to the

bipolar axis.

In paper I, we reported the results of mapping observations by several molecular lines (CO, HCN, and CS) using the Nobeyama 45-m radio telescope; the line profiles exhibit broad and/or narrow components depending on molecular species. We found that both broad and narrow components centered at  $V_{\text{lsr}} \simeq 35 \text{ km s}^{-1}$  are strongly peaked in intensity at the IRAS position of this source with a  $16''$  telescope beam. Without doubt, the broad component with a full width of more than  $20 \text{ km s}^{-1}$  must originate from the outflowing envelope of the central star. However, the spatial association of the narrow component to this object is a puzzle. The mass of the narrow component was estimated to be about  $10 M_\odot$  (within  $16''$  beam). The mass obtained is compatible with the core masses of dark clouds (for example, Fuller et al. 1991).

In this paper, we present a part of molecular-line observations toward this object, and discuss on it from a view point of circumstellar chemistry. In usual cases, molecular species found in dark clouds are considerably different from those found in the evolved objects [see, Glassgold (1996) and Ehrenfreund, Charnley (2000)]. Therefore, the origin of the cloud surrounding the central star of IRAS 19312+1950 can be resolved from this study in some degree. Although evidence of an evolved star is still not



**Fig. 1.** *JHK* false-color composite image of the field of IRAS 19312+1950, using the UH 88-inch telescope with the SIRIUS near-IR array camera (by courtesy of M. Tamura and K. Murakawa, National Astronomical Observatory). The image size is  $128'' \times 128''$ . The north is up, and the east is left.

**Table 1.** Telescope parameters (2001 March)

Receiver	Frequency (GHz)	HPBW ( $''$ )	Beam efficiency	Aperture efficiency
H22	22	72	0.81	0.62
S40	43	40	0.77	0.57
S100	86	18.6	0.49	0.42
S100	100	16.3	0.51	0.41
S100	110	15.4	0.48	0.35

completely crucial for this object or rather conflicting, we believe that this is a unique evolved object surrounded by a remnant of raw material. We present the observational results and discussion on the nature of this object in this paper.

## 2. Observations and results

The observations were made with the 45-m telescope at Nobeyama during 2001 February 4–9, and during 2002 December 11–21. A few additional observations were made on 2001 March 19 and 2002 May 19 for checking time variation of SiO maser line intensities. A cooled SIS-mixer receiver (S100) with a bandwidth of about 0.5 GHz were used, and the system temperature (including atmospheric noise) was 300–500 K (SSB) depending on the frequency and weather. In addition, HEMT and SIS-mixer receivers (H22 and S40) were used for the 22 GHz  $\text{H}_2\text{O}$  and the 43/49 GHz SiO/CS line observations, respectively. The half-power beam widths, and the aperture and beam efficiencies of the telescope at the observed frequencies were summarized in table 1. The antenna temperature ( $T_a^*$ ) given in the present paper is that corrected for the atmospheric and telescope ohmic loss but not for the beam nor aperture efficiency. Observations were made in a position switching mode, and the off-position was chosen  $12'$  away from the object in right ascension, where contamination by background CO emission was minimized. Further details of the observations were described in Paper I.

As described in Paper I, strong CO emission was seen toward this object. The  $15''$ -,  $30''$ -, and  $60''$ -grid mappings revealed that emission spikes at  $V_{\text{lsr}} = 27$ – $33$ , and

$43 \text{ km s}^{-1}$ , are extended more than a few arcmin, indicating that they are from fore/background clouds (see Paper I). We found that only the component at  $V_{\text{lsr}} = 37 \text{ km s}^{-1}$  is sharply peaked in intensity at the IRAS position ( $19^{\text{h}}31^{\text{m}}12^{\text{s}}.8$ ,  $19^{\circ}50' 22''$ , B1950). Mapping of line emissions of high density tracers, HCN,  $\text{HCO}^+$ , and CS, resulted in that the component at  $V_{\text{lsr}} = 35$ – $37 \text{ km s}^{-1}$  is sharply peaked also at the IRAS position of this source. In this paper, we only show a result of the 5-point  $1'$ -grid cross mapping in the  $\text{HCO}^+$   $J = 1$ – $0$  transition in figure 2. We can recognize from this figure that the  $\text{H}^{12}\text{CO}^+$   $J = 1$ – $0$  line consist of the two components: a narrow component at  $V_{\text{lsr}} = 37 \text{ km s}^{-1}$ , and the weak broad component spreading from  $V_{\text{lsr}} = 18 \text{ km s}^{-1}$  to  $50 \text{ km s}^{-1}$ . Because these two components are also found in the other molecular lines as CO, HCN, and SO, and because they are strongly concentrated on the IRAS position of this object, we conclude that they are not from the fore/background clouds. Because strong lines as the CO  $J = 1$ – $0$ ,  $^{13}\text{CO}$   $J = 1$ – $0$ ,  $\text{C}^{18}\text{O}$   $J = 1$ – $0$ , CS  $J = 2$ – $1$ , and HCN  $J = 1$ – $0$  (Paper I), are somewhat contaminated by emission from the back/foreground molecular clouds, we presented the result of the mapping by these lines separately in Paper I. The results for  $\text{HCO}^+$  described in this paper, i.e., the narrow and broad components and their spatial extensions, were completely confirmed by mm-wave interferometric observations using the BIMA array (Nakashima, Deguchi 2004)

### 2.1. Time variation of maser lines

We also observed maser lines to check their time variation. The results are summarized in table 2 and the line profiles are shown in figure 3. It was striking that the SiO  $J = 1$ – $0$   $v = 2$  spectrum in 2001 February–March (middle two panels in figure 3) exhibited strong emission at  $V_{\text{lsr}} \simeq 50 \text{ km s}^{-1}$ , but almost none in the  $J = 1$ – $0$   $v = 1$  and  $J = 2$ – $1$   $v = 1$  spectra. The integrated intensity of the SiO  $J = 2$ – $1$   $v = 1$  line increased by a factor of more than 3 in about 40 days in 2001 March. If we compare these line profiles with those taken in May 2000 [figure 2 in Nakashima, Deguchi (2000)], we can recognize drastic changes in the line profiles during 8 months. In May 2000, the radial velocities of most of maser lines were crowded around  $V_{\text{lsr}} \simeq 20 \text{ km s}^{-1}$ . However, we observed in 2001 February that they spread between  $V_{\text{lsr}} \simeq 20 \text{ km s}^{-1}$  and  $55 \text{ km s}^{-1}$ . This suggests that the center velocity of the

fig2.eps

**Fig. 2.** Line profiles of  $\text{HCO}^+$  and  $\text{H}^{13}\text{CO}^+$   $J = 1-0$  transitions. The observed position for each spectrum is indicated in the parentheses [ ( $\Delta\text{R.A.}$ ,  $\Delta\text{Dec.}$ ) relative to the IRAS position] on the right. The  $\text{HCO}^+$  profile at the center clearly shows broad ( $V_{\text{lsr}} = 20-50 \text{ km s}^{-1}$ ) and narrow (around  $V_{\text{lsr}} = 36 \text{ km s}^{-1}$ ) components.

star is  $\sim 37 \text{ km s}^{-1}$ , when we assume these maser lines are formed in the front and rear parts of the expanding shell.

Top two panels of figure 3 show a drastic time variation in  $\text{H}_2\text{O}$  maser profiles during one-year time span. In 2001 February, emission appeared around the stellar velocity,  $\sim 37 \text{ km s}^{-1}$ . While, after one year later, the profile looked doubly peaked and the line intensity became larger. Such a rapid change of the  $\text{H}_2\text{O}$  maser line profile between the groups A (single peak at stellar velocity) and group B (double peaks) in water masers (Engels et al. 1986) indicates that the direction of maser amplification changes in a short time (Deguchi 1977). If we assume that the double peaks of  $\text{H}_2\text{O}$  masers are emitted in the front and rear part of the expanding envelope, we can derive  $V_{\text{lsr}} = 33.6 \text{ km s}^{-1}$  for the systemic velocity and  $17.3 \text{ km s}^{-1}$  for the expansion velocity of the  $\text{H}_2\text{O}$  maser shell. The intensity of the lower velocity component tends to surpass that of the higher velocity component in circumstellar  $\text{H}_2\text{O}$  masers, indicating a maser amplification of continuum radiation of the central star (Takaba et al. 2001).

Emissions of OH 1612, 1665, 1667 MHz lines have been detected toward this object (Lewis 2000, private communication). Though the profiles of these OH lines are not exactly doubly peaked, emissions spread between  $V_{\text{lsr}} = 10$  and  $55 \text{ km s}^{-1}$ . This observation also suggests that the stellar velocity is around  $V_{\text{lsr}} \simeq 33 \text{ km s}^{-1}$ , which agrees with the stellar velocity derived from SiO and  $\text{H}_2\text{O}$  profiles within uncertainty.

## 2.2. Thermal lines of oxygen-bearing molecules

From the detections of SiO,  $\text{H}_2\text{O}$  and OH maser lines, we can safely suggest that the circumstellar envelope of this object is O-rich. However, the detections of  $\text{H}^{13}\text{CN}$   $J = 1-0$  line toward this object and the velocity shift to the maser lines (Nakashima, Deguchi 2000) puzzled us, and these facts yielded the argument if the thermal lines may be due to contamination by background.

To clarify the situation, we observed several oxygen-bearing molecules as SiO ( $J = 1-0$ ,  $v = 0$ ), SO,  $\text{SO}_2$ , and  $\text{HCO}^+$ . The results are summarized in table 3, and the line profiles are shown in figure 4. In addition, several lines of the various O-bearing molecules were searched for; frequencies of some transitions of these molecules were fallen in our spectrometer band coverages. We carefully checked whether or not any emission was seen in the spectra. These negative results are summarized in table 4.

The line profiles of these O-bearing molecules (except  $\text{H}^{13}\text{CO}^+$ ) are composed of two components: narrow sharp feature peaked at  $V_{\text{lsr}} \simeq 36 \text{ km s}^{-1}$ , and the broad feature with a full width at zero maximum of about  $30 \text{ km s}^{-1}$  (see figures 2 and 4). It seems that the SiO  $J = 2-1$   $v = 0$  line profile does not have any narrow component. For the case of the  $\text{SO}_2$  10(1,9)–10(0,10) line, the detection is marginal and it is difficult to tell whether it has the narrow or broad component.

It is well known that the profile of the optically thin line in the expanding shell is flat-topped and that of the thick line is parabolic when the telescope beam cannot resolve

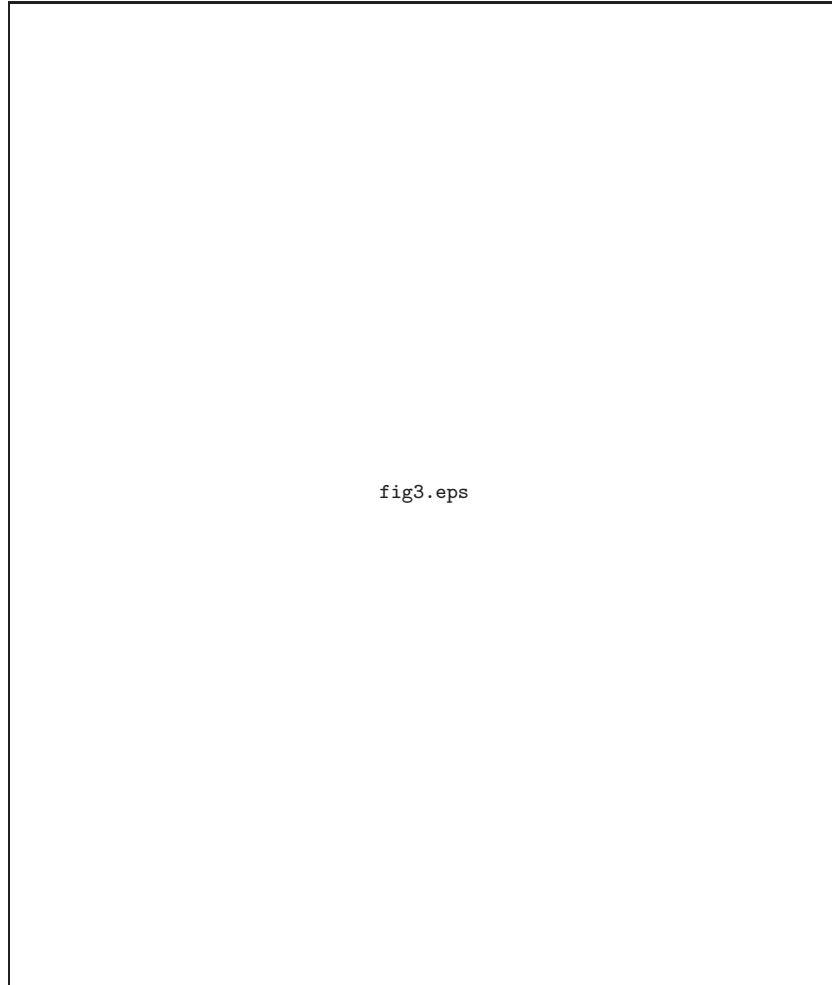


fig3.eps

**Fig. 3.** Time variation of the H<sub>2</sub>O and SiO maser lines. Dates of observations are shown in yymmdd format under the object name in each panel.

the envelope (Morris & Alcock 1977). The profiles of the broad components in figure 4 do not seem to be flat-topped, but rather they look like parabolic. Therefore, we fitted the profiles of the broad component by a parabolic line-shape function (excluding the narrow part of emission) and obtained the line parameters; the results are given in the 7–9 columns in table 3. The line parameters for the narrow components, which were computed from the residue by the parabolic fit, are also given in the last two columns in table 3.

The average center velocity of the broad components, 34.3 km s<sup>−1</sup>, is very slightly shifted from the average peak velocity of the narrow component, 35.6 km s<sup>−1</sup>. In addition the profile of the SiO thermal line ( $J = 2-1$   $v=0$ ) in figure 4 looks asymmetric with respect to the center velocity. The difference in the radial velocity between the narrow and board components seems significant. However, because the broad component is quite weak and overlapped with the narrow component, it is difficult to separate the broad component feature from the narrow component clearly in the present observations. Moreover, the profile of the CO  $J = 1-0$  line (top right panel of figure 1

of Paper I) clearly indicates a presence of absorptions on both high and low velocity sides of the narrow component, but with a slightly stronger absorption in the lower velocity side. Therefore, the difference of the center-velocity between the narrow and broad components could be due to radiation transfer effect (absorption at lower velocity side) by a weakly expanding part of the cloud with low excitation temperature (for example, Morris et al. 1985).

### 2.3. Thermal lines of C- and N-bearing molecules

We have also detected a number of lines of C- and N-bearing molecules. The results are summarized in table 5, and line profiles are shown in figures 5 and 6. These lines often have hyperfine splitting except the CS lines. The spectra of these lines do not seem to have the broad component but they exhibit the narrow component, although the hyperfine splitting (shown by arrows in figure 6) tends to conceal the presence of the broad component.

Line widths of narrow components at the half intensity maxima are approximately 1.5–2.0 km s<sup>−1</sup>. The average center velocity of these lines in table 5 is 35.9 km s<sup>−1</sup>, which is consistent with the average velocity of the narrow

**Table 2.** Time variations of maser line intensities.

Mol.	Frequency (GHz)	Transition	$V_{\text{lsr}}(\text{Peak})$ (km s <sup>-1</sup> )	$T_a^*(\text{Peak})$ (K)	$\text{Integ.Inten.}$ K (km s <sup>-1</sup> )	rms (K)	Obs.date (yyymmdd)
H <sub>2</sub> O	22.235	6(16)–5(23)	35.6	2.588	12.105	0.031	010210
H <sub>2</sub> O	22.235	6(16)–5(23)	16.3	6.628	12.526	0.323	021216
H <sub>2</sub> O	22.235	6(16)–5(23)	50.8	0.372	0.607	0.323	021216
SiO	43.122	1–0 $v=1$	41.1	0.108	0.122	0.021	010209
	42.821	1–0 $v=2$	49.9	0.184	0.817	0.021	010209
	86.243	2–1 $v=1$	36.9	0.184	0.513	0.020	010209
SiO	43.122	1–0 $v=1$	—	—	—	0.033	010319
	42.821	1–0 $v=2$	53.8	0.328	1.347	0.042	010319
	86.243	2–1 $v=1$	23.2	0.199	1.731	0.020	010319
SiO	43.122	1–0 $v=1$	51.8	0.213	0.376	0.055	020519
	42.821	1–0 $v=2$	51.0	0.414	1.036	0.067	020519
SiO	43.122	1–0 $v=1$	50.8	0.186	0.346	0.030	021215
	42.821	1–0 $v=2$	51.7	0.420	0.970	0.043	021215

**Table 3.** Line parameters for line with broad and narrow features

Mol.	Freq. (GHz)	Transition	peak feature			broad compo.			narrow compo.	
			$V_{\text{lsr}}(\text{p})$ (km s <sup>-1</sup> )	$T_a^*(\text{p})$ (K)	rms (K)	$V_{\text{lsr}}(\text{par})$ (km s <sup>-1</sup> )	$T_a^*(\text{par})$ (K)	FWZM (km s <sup>-1</sup> )	$T_a^*(\text{nar})$ (K)	I.I.(nar) (K km s <sup>-1</sup> )
SiO	86.847	2–0 $v=0$	33.3	0.128	0.027	35.1	0.086	34.9	—	—
H <sup>13</sup> CO <sup>+</sup>	86.754	1–0	36.2	0.123	0.021	—	—	—	0.123	0.556
HCO <sup>+</sup>	89.189	1–0	36.9	0.326	0.025	32.3	0.060	41.8	0.269	0.849
SO	99.300	3(2)–2(1)	35.8	0.624	0.019	33.5	0.112	44.5	0.513	2.459
	109.252	2(3)–1(2)	35.6	0.104	0.043	36.2	0.028	35.2	0.076	0.093
	100.030	4(5)–4(4)	—	—	0.023	—	—	—	—	—
SO <sub>2</sub>	104.239	10(1,9)–10(0,10)	35.8	0.040	0.012	—	—	—	—	—

**Table 4.** Negative results for S-bearing molecules

Mol.	Freq. (GHz)	Transition	rms (K)
SO <sub>2</sub>	86.153	39(9,31)–40(8,32)	0.016
	86.639	8(3,5)–9(2,8)	0.025
	90.548	25(3,23)–24(4,20)	0.049
	104.029	3(1,3)–2(0,2)	0.020
<sup>34</sup> SO <sub>2</sub>	88.720	7(3,5)–8(2,9)	0.042
	104.391	10(1,9)–10(0,10)	0.025
<sup>34</sup> SO	97.715	3(2)–2(1)	0.063
OCS	109.463	9–8	0.023
SiS	90.771	5–4	0.058
C <sup>33</sup> S	48.585	1–0	0.033
C <sup>34</sup> S	48.206	1–0	0.027

component of O-bearing molecules. The width of the narrow component seems to vary from molecule to molecule. The CS line has a full width of about 8 km s<sup>-1</sup>, while, HCO<sup>+</sup> less than 2 km s<sup>-1</sup>. This fact can be interpreted by a characteristic of the lines formed in a turbulent media where the width depends on the line optical depth [for example, see Park & Hong (1995)].

The molecular species exhibiting the narrow component are somewhat similar to those observed in the C-rich circumstellar envelopes (e.g., Bujarrabal et al. 1994). A number of carbon-chain molecules have been detected in the C-rich protoplanetary nebulae (Fukasaku et al. 1994). However, SiS, which is common in the C-rich envelopes, was not detected in IRAS 19312+1950.

The high HNC/HCN abundance ratio is often considered as a signature of photochemical reactions (Morris et al. 1987; Glassgold 1996). The line intensity of the HNC emission,  $T_a^* \sim 0.6$  K, is comparable with the HCN intensity,  $T_a^* \sim 0.6$  K in this object, suggesting a photochemical origin of this molecule. Even taking into account the line saturation in the HCN lines [ $\tau(F=2-1) \sim 2-4$  can be deduced from  $T_a^*(F=0-1)/T_a^*(F=2-1) = 0.56$  and  $T_a^*(F=1-1)/T_a^*(F=2-1) = 0.76$  in this star, where



**Table 5.** Line parameters for species with narrow features only

Mol.	Freq. (GHz)	Transition	$V_{\text{lsr}}(\text{peak})$ (km s <sup>-1</sup> )	$T_a^*(\text{peak})$ (K)	Integ.Int. (K km s <sup>-1</sup> )	rms (K)
NH <sub>3</sub>	23.694	(1,1)	35.1	0.091	0.731	0.012
	23.723	(2,2)	37.4	0.041	0.203	0.010
	23.870	(3,3)	—	—	—	0.010
	24.139	(4,4)	—	—	—	0.022
CS	48.991	1–0	36.2	0.621	1.977	0.042
	97.981	2–1	36.3	1.100	3.852	0.059
C <sup>34</sup> S	96.413	2–1	35.8	0.191	0.441	0.0118
H <sub>2</sub> CS	104.617	3(1,2)–(2(1,1)	35.1	0.046	0.313	0.010
HNC	90.600	1–0	35.4	0.581	1.930	0.039
N <sub>2</sub> H <sup>+</sup>	93.174	1–0	34.1	0.122	0.657	0.020
HC <sub>3</sub> N	100.076	11–10	36.3	0.163	0.481	0.018
HC <sub>3</sub> N	109.174	12–11	36.2	0.104	0.403	0.020
CN	113.491	1-0 (all)	36.7	0.521	3.439	0.033
CH <sub>3</sub> OH	96.739	2(–1)–1(1) E	35.4	0.142	0.384	0.018
CH <sub>3</sub> OH	96.741	2(0)–1(0) A+	35.9	0.159	0.448	0.018
C <sup>17</sup> O	112.359	1–0 (+hyperfine)	35.5	0.197	1.101	0.027
<sup>13</sup> C <sup>18</sup> O	104.711	1–0	36.4	0.045	0.200	0.010

these ratios are 0.2 and 0.6, respectively, in a thermal equilibrium], we can reach the same conclusion that the HNC/HCN abundance ratio is relatively high ( $> 0.3$ ) in the narrow component.

The molecular species exhibiting the narrow component are also similar to those found in the dark clouds; NH<sub>3</sub>, SO, H<sub>2</sub>CS, and CH<sub>3</sub>OH, etc., were observed in LDN 134N [see Dickens et al. (2000)]. Therefore, in order to check the similarity in molecular abundances to dark clouds, we also searched for H<sub>2</sub>CS and CH<sub>3</sub>OH. We found emission from these molecules and the line profiles are shown in the bottom panels of figures 5 and 6.

### 3. Discussion

Paper I estimated the distance to this object as 2.5 kpc; the bolometric correction for the IRAS 12 micron flux density,  $(BC)_{12} = 3.8$  (Deguchi et al. (2001)), was applied from the  $R$  (DSS),  $J$ ,  $H$ , and  $K$  (2MASS) magnitudes and IRAS 12, 25, 60, and 100  $\mu\text{m}$  flux densities, and typical luminosity of the AGB object,  $8000 L_{\odot}$ , was used. For simplicity, we adopt this value for a distance of this object in this paper.

Paper I gave two reasons for the central star to be an evolved object: (1) the presence of deep CO first overtone absorption bands at 2.3  $\mu\text{m}$  as usually seen in late MIII stars, and (2) no nearby starforming activity such as often seen in YSOs. Furthermore, we can add the OH maser line property of this object: the dominant OH 1612 MHz line accompanying weak OH 1665/1667 HMz lines (Lewis 2001; private communication), which is often used to separate evolved objects from YSOs (Caswell 2000). All of

these facts strongly support the evolved star interpretation of the central star.

There is evidence for O-rich material surrounding a class of carbon stars (Willems, de Jong 1986; Nakada et al. 1987; Le Bertre et al. 1990; Jiang 2000). These materials are considered to be the gas and dust which were ejected in the O-rich AGB era of the central star, but were trapped by a hypothetical binary companion (Lloyd-Evans 1990). When the central star changes the atmospheric composition from O-rich to C-rich, the presence of the O-rich material would observationally become evident due to their chemistry difference. In fact, a sharp narrow CO line profile ( $\sim 1 \text{ km s}^{-1}$ ) having slightly broader wing emission ( $\sim 5 \text{ km s}^{-1}$ ), which is similar to the narrow and broad components of IRAS 19312+1950, has been found in the silicate carbon star, BM Gem (Kahane et al. 1998; Jura, Kahane 1999). In order to explain O-rich materials surrounding silicate carbon stars, a model of orbiting molecular reservoirs has been proposed (Lloyd-Evans 1990; Jura, Kahane 1999). In contrast, Kerschbaum et al. (1999) found O-rich examples (semiregular and irregular variables) of the narrow ( $\lesssim 5 \text{ km s}^{-1}$ ) feature superposed on the broad ( $\sim 20 \text{ km s}^{-1}$ ) component in CO lines. These may be interpreted as a result of either multiple winds or a Keplerian disk (Bergman et al. 2000).

It is possible that we are looking these trapped materials as a narrow-component cloud [for example, Kahane et al. (1998)]. Because the narrow and broad components found in the IRAS 19312+1950 line profiles have a similarity with the CO line features found in these stars, the model of orbiting molecular reservoirs must be pursued first in the present case too. However, as discussed in

**Table 6.** Negative results for miscellaneous species

Molecule	Frequency (GHz)	Transition	rms (K)	Freq.	Ref.
MgNC	23.859	2-1-	0.006	Kawaguchi et al.	1993
	23.875	2-1+	0.006	Kawaguchi et al.	1993
	47.726	4-3-	0.023	Kawaguchi et al.	1993
	47.741	4-3+	0.023	Kawaguchi et al.	1993
	95.454	$N=8-7-$	0.016	Guelin et al.	1995
	95.469	$N=8-7+$	0.016	Guelin et al.	1995
$^{26}\text{AlCl}$	89.351	6-5	0.016	calc. from Guelin et al.	(1995)
	104.237	7-6	0.013	calc. from Guelin et al.	(1995)
$\text{CH}_3\text{OH}$	48.372	1(0)-0(0) A+	0.028	Lovas	1992
	48.376	1(0)-0(0) A+	0.028	Lovas	1992
$\text{C}_4\text{H}$	104.667	11-10 $J=23/2-21/2$	0.010	Lovas	1992
	104.705	11-10 $J=21/2-19/2$	0.010	Lovas	1992
$\text{H}_2\text{O}$	96.261	4(4,0)-5(3,3) $\nu_2=1$	0.018	Lovas	1992

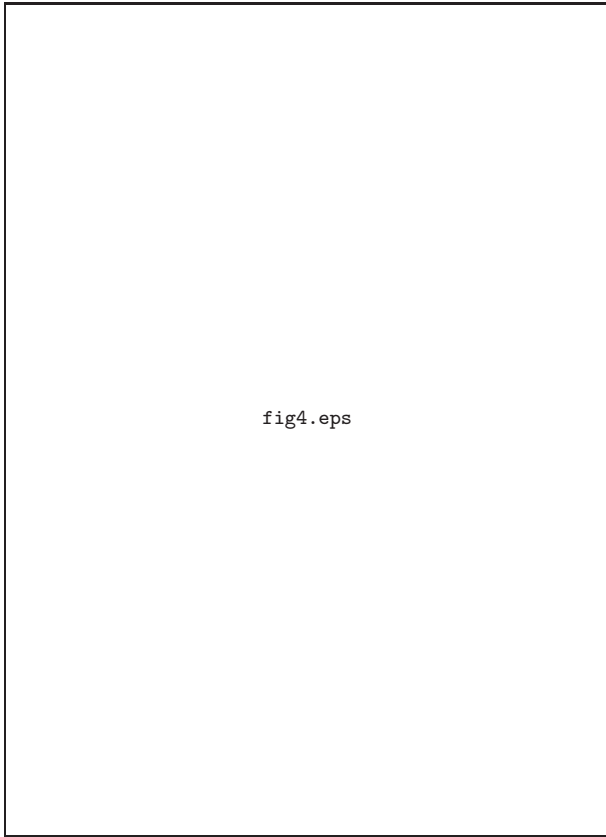


**Fig. 4.** Line profiles of SiO  $J=2-1$   $v=0$ , SO  $3(2)-2(1)$  and  $2(3)-1(2)$ , and SO<sub>2</sub>  $10(1,9)-10(0,10)$  transitions. The SiO profile exhibits only a broad component, and SO profiles exhibit both broad and narrow components. Because of the noise, it is hard to judge whether it is a narrow or broad component for SO<sub>2</sub>.

the following sections, the derived total mass of the gas ( $\sim 25 M_{\odot}$  within  $15''$  radius), which is necessary to explain the narrow component of IRAS 19312+1950, seems too large as an orbiting molecular reservoir.

### 3.1. The broad component: molecular abundances

In order to obtain molecular abundances, numerical calculations based on the large-velocity-gradient (LVG) model were performed. Here the broad-component emission was assumed to come from the expanding envelope of an AGB/post-AGB object. The numerical code developed by Deguchi et al. (1990) was used to compute line intensities of linear molecules in the expanding shell. The code was modified to involve SO molecule which has a slightly complex energy-level structure; transition probabilities (Einstein A coefficients etc.) of SO were taken from Tiemann (1974) [see the level diagram in Omont et al. (1993)]. In this numerical code, the kinetic temperature of the envelope is calculated by taking into account the adiabatic and line (CO, CI, and CII) cooling and the gas-dust drift and CI ionization heating (see the detail in Deguchi et al. 1990). Dissociations of CO, HCN, SiO, and SO due to interstellar UV radiation are taken into account; self absorptions of CO UV lines are also taken into account. However, photodissociation rates of SiO and SO are not well known. Therefore, we assumed that the photodissociation rates are the same as the CO dissociation rate (without self-absorption).

We assumed that the envelope is expanding with a constant velocity of  $25 \text{ km s}^{-1}$ . The calculation starts from the inner radius of  $1.5 \times 10^{16} \text{ cm}$  and stops at the outer radius of  $1.87 \times 10^{17} \text{ cm}$  (corresponding to a  $5''$  radius from the central star). The mass loss rate (to be constant), kinetic temperature at the inner radius, and molecular abundance were free parameters and the best-fit model to the observational data was sought. The results are given in table 7, where molecular species, abundance of the observed molecule with the broad component, frequencies, transitions, and the observed main-beam brightness temperature, and the calculated main-

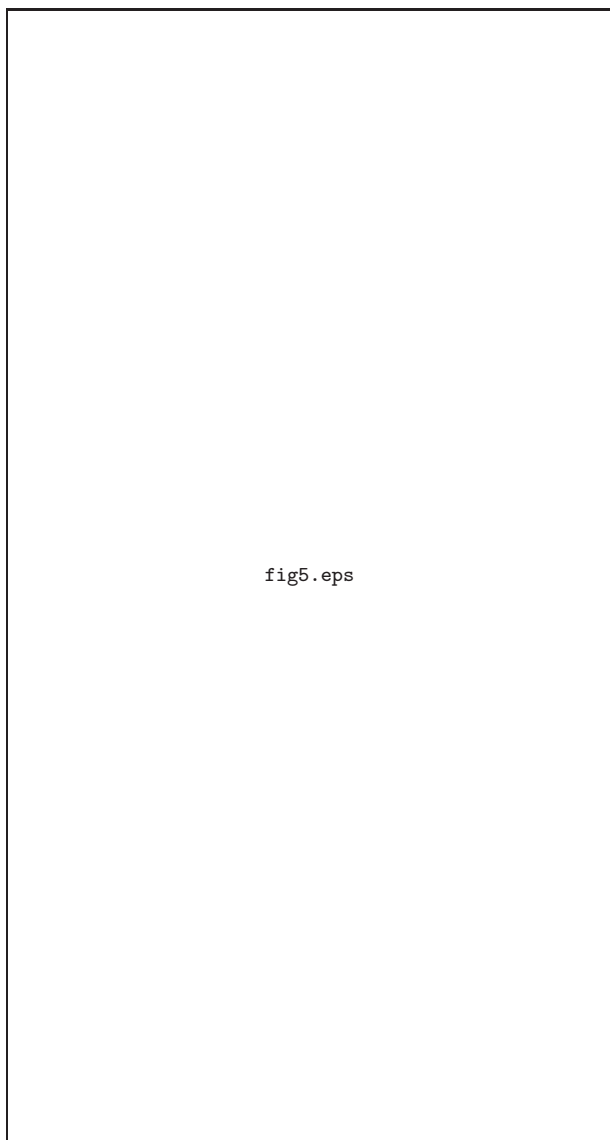


**Fig. 5.** Line profiles of  $\text{HC}_3\text{N}$ ,  $\text{CS}$  and  $\text{H}_2\text{CS}$ . The hyperfine splitting of  $\text{HC}_3\text{N}$  is quite small and not recognizable here. Both of  $\text{HC}_3\text{N}$  and  $\text{CS}$  lines seem to exhibit a narrow component.

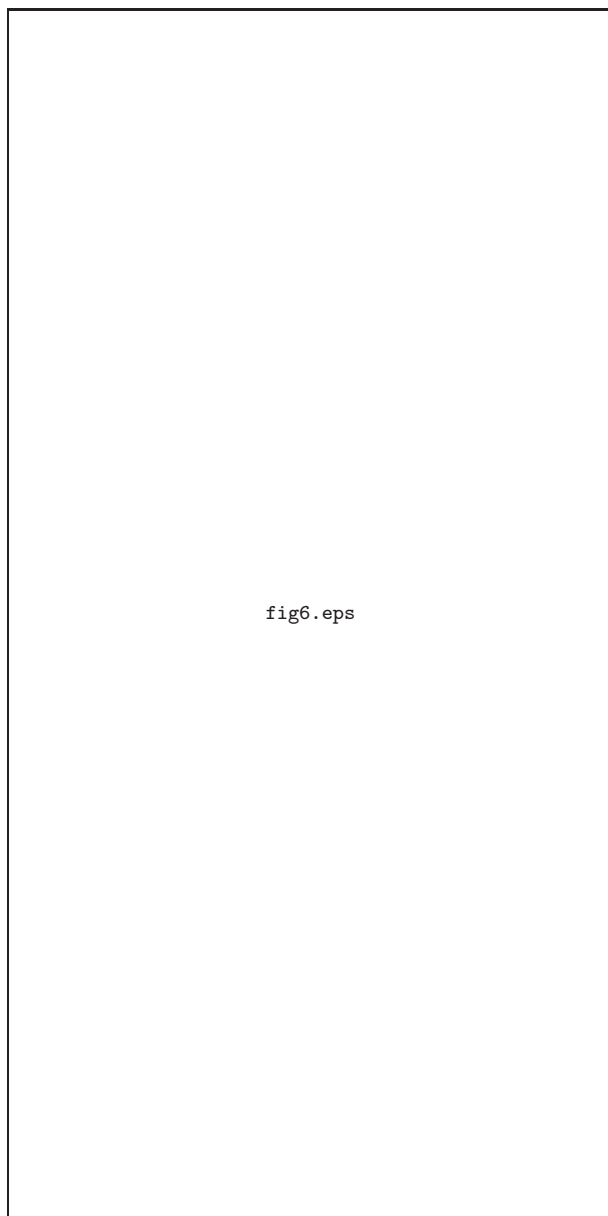


**Fig. 6.** Line profiles of  $\text{NH}_3$ ,  $\text{HNC}$ ,  $\text{N}_2\text{H}^+$ , and  $\text{CH}_3\text{OH}$ . The positions of the hyperfine lines were indicated by arrows. The splitting of  $\text{HNC}$  are less than  $0.7 \text{ km s}^{-1}$ , so that they are not shown here. All of these lines exhibits only a narrow components.



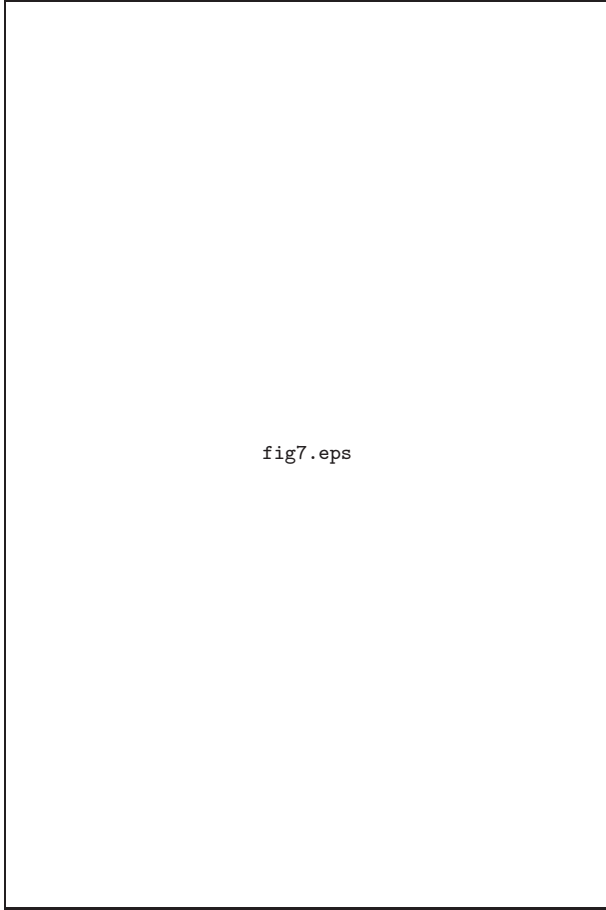


**Fig. 7.** Line profiles of  $\text{NH}_3$ ,  $\text{C}^{34}\text{S}$ ,  $\text{C}^{17}\text{O}$ , and  $^{13}\text{C}^{18}\text{O}$  lines.

beam brightness temperature were shown for the model with the mass loss rate of  $2.6 \times 10^{-4} M_{\odot} \text{ yr}^{-1}$ . In this model, the main-beam brightness temperature was determined mostly from line brightness temperature at around  $10^{17} \text{ cm}$  with  $N_{\text{H}_2} = 1.1 \times 10^4 \text{ cm}^{-3}$  (except the  $\text{CO } J=1-0$  transition). Because photodissociation of molecules occurs slightly outside of this radius, a slight uncertainty of the photodissociation rate in various molecules except  $\text{CO}$  does not influence much to the results. The obtained  $\text{SO}$  abundance,  $5.5 \times 10^{-7}$ , is similar to those found in normal O-rich envelopes (Guilloteau et al. 1986; Omont et al. 1993).

For the case of  $\text{HCO}^+$ , the abundance of this molecule is assumed to be constant through the envelope in the present calculation. Because the molecular abundances of  $\text{HCN}$  and  $\text{HCO}^+$  in the O-rich circumstellar envelopes were somewhat controversial (Morris et al. 1987; Deguchi et al. 1990), we also computed the expected  $\text{HCO}^+$  abundance in the same code used in Deguchi et al. (1990). The maximum  $\text{HCO}^+$  abundance can reach to  $1.5 \times 10^{-5}$  per  $\text{H}_2$  at the radius  $2.3 \times 10^{17} \text{ cm}$  (if mass loss occurs continuously beyond  $1.87 \times 10^{17} \text{ cm}$ ). Because there are still some arguments in the  $\text{H}_3^+$  dissociative recombination rate (Amano 1988), this value is probably available maximum. The obtained  $\text{HCO}^+$  abundance is less than the value ob-

**Table 7.** Model fit for the broad component for mass loss rate of  $2.6 \times 10^{-4} M_{\odot} \text{ yr}^{-1}$

Mol.	Abundance (per $\text{H}_2$ )	Frequency (GHz)	Transition	$T_{\text{MB}}^{\text{obs}}$ (K)	$T_{\text{MB}}^{\text{model}}$ (K)
$\text{SiO}$	$1.1 \times 10^{-7}$	86.847	2-1 $v=0$	0.18	0.18
$\text{HCN}$	$3.9 \times 10^{-7}$	88.632	1-0	0.41	0.41
$\text{HCO}^+$	$5.7 \times 10^{-8}$	89.188	1-0	0.12	0.12
$^{13}\text{CO}$	$4.0 \times 10^{-6}$	110.201	1-0	< 0.1	0.09
$\text{CO}$	$1.3 \times 10^{-4}$	115.271	1-0	1.79	1.79
$\text{SO}$	$5.5 \times 10^{-7}$	86.094	2(2)-1(1)	0.05	0.04
		99.299	3(2)-2(1)	0.22	0.20
		109.252	2(3)-1(2)	0.05	0.10

tained from the present photo-chemical model (see also Glassgold 1996). Furthermore, clumpiness in the outflowing envelope strongly influences the photo-chemical products (Redman et al. 2003). The spherical model with outer radius of  $1.87 \times 10^{17} \text{ cm}$  may be inadequate for explaining  $\text{HCO}^+$ . In fact, a bipolar structure has been found for the  $\text{HCO}^+$  emission distribution (Nakashima, Deguchi 2004).

### 3.2. The narrow-component cloud: molecular abundance

In order to obtain molecular abundances in the narrow component cloud, we performed numerical calculations under the LVG model. Though the LVG model was a choice for a matter of convenience here, more sophisticated, but formidable radiative-transfer model involving clumpiness and turbulence with velocity gradient (Park & Hong 1995) must be pursued for the narrow component cloud as a next step; there is evidence that the spectral line of the narrow component is broadened by turbulence as mentioned in section 2.3. However, the present data, which was obtained in a single-dish observation, do not provide much information on spatial distribution of molecular emission. Then, it seems meaningless to argue on differences of outcomes between the LVG and turbulence models. Therefore, we used the LVG model for the narrow component cloud with inner and outer radii,  $1.87 \times 10^{17} \text{ cm}$  and  $5.6 \times 10^{17} \text{ cm}$  (corresponding to 5 and  $15''$  radii), respectively. The uniform expansion rate,  $dV/dr = 3.2 \times 10^{-13} \text{ s}^{-1}$ , was adopted giving an expansion velocity of  $2 \text{ km s}^{-1}$  at the outer boundary. Radiative interaction with the central expanding core (broad component) was also taken into account as if the core emits continuum emission, but it turned out to be negligible. The number density was assumed to decrease with radius as  $r^{-3}$ , and the absolute value of the density and the molecular abundances were adjusted to fit calculated to observed line intensities. For simplicity, the calculations were restricted for linear-type molecules (except  $\text{SO}$ ). We solved level populations up to  $J=6$  for  $\text{CO}$ ,  $\text{HCN}$ ,  $\text{HCO}^+$ , and  $\text{HNC}$ , to  $J=8$  for  $\text{CS}$ , and to  $J=15$  for  $\text{HC}_3\text{N}$  at different radii and calculated the brightness temperatures. Multiplying the telescope beam pattern, we obtained the molecular abundances to fit the calculated to the main-beam brightness temperatures of observed lines. Kinetic

**Table 8.** Molecular abundance for narrow component

Molecule	Abundance (per H <sub>2</sub> )	Freq. (GHz)	Transition (K)	$T_{MB}^{\text{obs}}$ (K)	$T_{MB}^{\text{calc}}$ (K)
CO	$1.3 \times 10^{-4}$	115.271	1–0	6.83	6.83
HCN	$4.0 \times 10^{-9}$	88.631	1–0	0.77	0.77
HCO <sup>+</sup>	$1.2 \times 10^{-9}$	89.189	1–0	0.53	0.53
HNC	$3.4 \times 10^{-9}$	90.663	1–0	1.12	1.12
HC <sub>3</sub> N	$7.0 \times 10^{-9}$	100.076	11–10	0.31	0.31
		109.174	12–11	0.19	0.22
CS	$1.0 \times 10^{-8}$	48.991	1–0	0.85	1.23
		97.981	2–1	1.77	1.66
SO	$5.5 \times 10^{-9}$	86.094	2(2)–1(1)	0.05	0.27
		99.300	3(2)–2(1)	0.77	0.77
		109.252	2(3)–1(2)	0.17	0.42

temperature in the model (uniform) was determined to be 13 K by adjusting the calculated <sup>12</sup>CO line intensity to the observed intensity. The results are shown in table 8. It suggests that the abundances of HCN and SO are two orders of magnitude lower than those for the broad component (table 7), making the discrete difference of the molecular composition at the boundary between narrow and broad components. The total mass of the narrow component cloud in this model is  $24.4 M_{\odot}$  (within 15'' radius), which is consistent with the previous estimation of the mass of this dust cloud based on a <sup>18</sup>CO column density (Nakashima et al. 2004).

### 3.3. isotopic abundance

Another important clue to guess the origin of cool material surrounding the object is isotopic abundance. For this purpose, we obtained the isotope abundance ratios for the narrow-component cloud with the same LVG model used in the previous section. Table 9 summarizes the isotope line-intensity (peak-intensity) ratios and calculated abundance ratios (in the 2nd and 5th columns, respectively). For comparison, terrestrial and interstellar isotope abundance ratios are given in the last two columns. If lines are optically thin, the line intensity ratio approximately gives the isotope abundance ratio. However, because strong lines, as <sup>13</sup>CO  $J=1-0$ , HCO<sup>+</sup>  $J=1-0$  and CS  $J=2-1$ , tend to be saturated in intensity (optically thick), they only give a lower limit of abundance ratio.

The ratio, C<sup>18</sup>O/<sup>13</sup>C<sup>18</sup>O, is very often regarded to give the <sup>12</sup>C/<sup>13</sup>C abundance ratio in dark clouds in a good approximation [for example, see Langer, Penzias (1993)] because these lines are optically thin. In fact, in the LVG model computations, the line intensities of the minor CO isotopic species vary almost proportional to the abundance of CO [times  $(dV/dr)^{-1}$  too] [e.g., figure 17 of Castets et al. (1990)], as far as it is optically thin. We obtained the ratio <sup>12</sup>C/<sup>13</sup>C  $\sim 27 \pm 9$  from the C<sup>18</sup>O/<sup>13</sup>C<sup>18</sup>O line ratio in table 9. It is well known that <sup>13</sup>C is enriched in envelopes of some carbon stars [for example, see Woods et al. (2003)]. Furthermore, Jura et al. (1988) found low line

intensity ratio of <sup>12</sup>CO to <sup>13</sup>CO  $J=1-0$  transition in several optical carbon stars which exhibit <sup>13</sup>C-richness. The observed abundance ratios are approximately between 3 and 80 for evolved objects [for example, Schöer, Olofsson (2000)]. No enrichment of <sup>13</sup>C compared with the case of interstellar clouds (in table 9) indicates that the material is unlikely to be an ejecta from a (supposedly) dead, C-rich AGB companion.

However, we have to remind that the detection of <sup>13</sup>C<sup>18</sup>O  $J=1-0$  line was marginal (see the lowest panel of figure 7). Taking into account the uncertainty of the temperature calibration and pointing errors of the 45-m telescope at 110 GHz due to wind etc., we think that the observed value involves uncertainty of a factor of about 2. Furthermore, if we consider the model dependency of the CO line intensity, especially in turbulent clumpy clouds, and of emission size difference in C<sup>18</sup>O and <sup>13</sup>C<sup>18</sup>O lines, we think that the conclusion is somewhat provisional.

Kahane et al. (1992) observed several carbon stars and planetary nebulae, and found that the <sup>18</sup>O/<sup>17</sup>O ratio is less than unity. However, the present case is apparently different from such C-rich objects; the C<sup>18</sup>O/C<sup>17</sup>O  $\sim 5$  in table 9. Concerning on <sup>17</sup>O, we can safely conclude that it is not appreciably enriched in the narrow-component cloud as in these C-rich objects. Rather, the <sup>18</sup>O/<sup>17</sup>O ratio coincides with the interstellar value. In conclusion, we found no evidence of the isotope enrichment/deficiency compared with the interstellar values in the present observation.

### 3.4. Narrow component: what is it ?

The detections of SO, HCN, HCO<sup>+</sup>, and NH<sub>3</sub> first suggested a resemblance of chemistry between IRAS 19312+1950 and OH231.8+4.2 (a proto-planetary nebula), leading a conclusion that IRAS 19312+1950 was a protoplanetary nebula. In fact, the first three molecules were observed to have a broad component as well. However, we recognized several differences between the molecular species found in IRAS 19312+1950 and OH231.8+4.2. Firstly, SO<sub>2</sub> molecules are quite deficient

**Table 9.** Isotope line-intensity and abundance ratio (narrow component)

Molecule	Peak I. ratio	Uncertainty	Transition	Calc. abu. ratio	Terrestrial ratio <sup>1</sup>	Interstellar ratio
$^{13}\text{CO}/^{13}\text{C}^{18}\text{O}$	66	$\pm 20$	1-0	498	489	489 <sup>2</sup>
$^{13}\text{CO}/\text{C}^{18}\text{O}$	3.6	$\pm 0.3$	1-0	19	5.43	7-25 <sup>3</sup>
$\text{C}^{18}\text{O}/^{13}\text{C}^{18}\text{O}$	18	$\pm 6$	1-0	27	89.1	20-70 <sup>4</sup>
$\text{C}^{18}\text{O}/\text{C}^{17}\text{O}$	4.1	$\pm 0.7$	1-0	5.7	5.5	3.2 <sup>2</sup>
$\text{HCO}^+/\text{H}^{13}\text{CO}^+$	2.2	$\pm 0.5$	1-0	10	89.1	$\sim 50$ <sup>5</sup>
$\text{CS}/\text{C}^{34}\text{S}$	4.8	$\pm 1.0$	2-1	9.1	22.5	24 <sup>5</sup>

<sup>1</sup> from appendix VII of Townes, Shawlow (1975).

<sup>2</sup> Wilson, Matteucci (1992)

<sup>3</sup> Gredel et al. (1994)

<sup>4</sup> Langer, Penzias (1993), Savege et al. 2002; see references therein.

<sup>5</sup> Lucas (1998)

<sup>6</sup> Chin et al. (1996)

in IRAS 19312+1950 (see table 4), but were abundant in OH231.8+4.2 (Morris et al. 1987), although SO lines are detected in both. The line intensity ratio of the SO<sub>2</sub> 3(13)–2(02) (104.029 GHz) to SO 2(2)–1(1) line (86.094 GHz) is 6.2 in OH231.8+4.2 (Morris et al. 1987); the abundance ratio of SO<sub>2</sub> to SO is about 4–7 (Claude et al. 2000), and somewhat similar values have also been found in O-rich AGB stars (Sahai, Wannier 1992) (except 2 supergiants, NML Cyg and VY CMa, which seem to be SO<sub>2</sub>-poor relative to SO; Omont et al. 1993). However, this intensity ratio is  $\lesssim 0.2$  in IRAS 19312+1950 (in the condition that the marginally detected SO<sub>2</sub> line is regarded to be a narrow component). The deficiency of SO<sub>2</sub> relative to SO in IRAS 19312+1950 could be attributed to a difference in O/C abundance ratio between two stars, or to less development of shock compared with OH231.8+4.2 (e.g., Claude et al. 2000). Secondly, the NH<sub>3</sub> (1,1) and (2,2) inversion lines were detected in IRAS 19312+1950. The line intensity ratio suggests the rotational temperature of the concerning levels (both para-NH<sub>3</sub>) of 19 K for the narrow component cloud. For the case of OH 231.8+4.2, the line intensities suggested the NH<sub>3</sub> rotational temperature of  $(27 \pm 4)$  K (Morris et al. 1987), indicating that the narrow-component cloud is slightly cooler than the envelope of OH231.8+4.2.

Rich molecular lines detected toward IRAS 19312+1950 (as a narrow component) rather resemble to the lines usually found in dark clouds. For example, in L134N, the SO lines have been found to be strong but not much SO<sub>2</sub> (Swade 1989; Dickens et al. 2000). Therefore, the deficiency of SO<sub>2</sub> to SO can be explained naturally if we consider that the narrow-component cloud is a dark cloud as L134N.

The detection of CH<sub>3</sub>OH in this paper also favors the dark-cloud interpretation of the narrow component cloud. The detected CH<sub>3</sub>OH lines at 96.74 GHz are thermal emission and have been found widely in dark (Friberg et al. 1988) and translucent clouds (Turner 1998). Note that a search for the 6.7 GHz CH<sub>3</sub>OH 5<sub>1</sub>–6<sub>0</sub> A<sup>+</sup> line, one of the strongest CH<sub>3</sub>OH maser lines, has been negative in IRAS 19312+1950 (MacLeod et al. 1998; Szymczak et

al. 2000), although numerous maser lines of CH<sub>3</sub>OH have been detected normally in dense massive star forming clouds (in this sense, the cloud toward IRAS 19312+1950 is not a massive star forming region). Though CH<sub>3</sub>OH could be produced in circumstellar envelopes of O-rich stars (Charnley et al. 1995), it has never been detected in evolved stars to the authors' knowledge [see Latter, Chanley (1996) ; Charnley, Latter (1997)].

Time-dependent chemical models of low-mass dark-cloud cores (Nejad, Wagenblast 1999) gave a result that abundances of C-bearing complex molecules as CH<sub>3</sub>OH and CH<sub>3</sub>CN are peaked at a few times 10<sup>5</sup> years, while the peak abundance of SO and SO<sub>2</sub> are attained at later times of  $\sim 10^6$  years (though these time scales are dependent on the density of the cloud). Note that the chemistry of CH<sub>3</sub>OH and CH<sub>3</sub>CN in translucent clouds is still quite controversial [see an excellent summary in Turner (1998) on gas-phase and grain-surface chemistry], and the confinement of their chemical evolution at relatively earlier time in the Nejad, Wagenblast (1999)'s model was critically affected by cosmic-ray-induced photoionization and photodissociation processes.

It is useful to compare the time scale of molecule formation with the other physical time scales of the envelope. The time scale of expanding gas with 10 km s<sup>−1</sup> crossing the envelope ( $15'' \sim 5.8 \times 10^{17}$  cm) is as short as  $1.8 \times 10^4$  y. Therefore, even if we interpret the narrow-component cloud being the stellar ejecta, we need relatively long-lived ( $\sim 10^6$  years) trapped materials to create CH<sub>3</sub>OH. The period of circulation around a 5  $M_{\odot}$  star at 10'' radius is  $1.8 \times 10^6$  y. Therefore, it is possible to create the complex molecules as CH<sub>3</sub>OH within one orbital motion of ejected gas. Because the life time of the thermal-pulse AGB era is  $\lesssim 10^6$  y for a progenitor mass of  $> 4 M_{\odot}$  (Blöcker 1995), the ejecta must come from the companion, not from the AGB/post-AGB star which is seen now as a central star of the mass of about 5  $M_{\odot}$  (Paper I).

It is possible to consider that material of the narrow-component cloud is a remnant of the dark cloud which encountered with this object several million years ago. Such encounter with a dark cloud is considered to occur rela-

tively frequently in the solar neighborhood (in every  $\sim 10$  Myr per a star; Griv et al. 1997; Fresneau et al. 2003). Taking into account the chemical-evolution time scale of dark clouds, we estimate that such encounter must have occurred in the last  $10^6$  yr ago for IRAS 19312+1950. In this case, the encountered cloud cannot be very far away from the object at present; for example, it must be located within  $5'$  from IRAS 19312+1950, provided that the relative velocity between the star and the cloud is  $10 \text{ km s}^{-1}$ . This is also an attractive hypothesis in view of an explanation for silicate carbon stars and narrow CO line profiles of short-period variable stars. However, the large mass of the narrow-component material (as much as  $\sim 20 M_{\odot}$ ) again causes a problem in this interpretation; It must be quite difficult to accrete the mass more than the star mass during the passage of such dark cloud and to keep it around the object during a few Myr.

Note that brightness of the central star at near-infrared bands ( $K = 6.3$  in IRAS 19312+1950 ; Paper I) is so different from class-0 YSOs as L134N or L1551 IRS5. These objects usually do not have any bright near-infrared counterparts. For example, L1551 IRS5 does show very faint patchy structure in the K-band images [Hodapp 1994; or see Momose et al. (1998) for the overlay image with the  $\text{C}^{18}\text{O } J=1-0$  map]. As far as we see 2MASS images of the similar type of objects as L134N (Dickens et al. 2000) and IRAS 16293–2422 (Blake et al. 1994), we find no near-infrared counterpart. Though HH objects as B5 IRS 1 (Fuller et al. 1991;  $K=11.21$ ) tend to have brighter near-infrared counter parts (Reipurth, Bally 2001), these objects have well developed CO outflow too. On the other hand, the size of high-velocity flow of IRAS 19312+1950 (if the broad component is interpreted as a bipolar flow observed in YSOs) is small compared with the size of narrow component cloud ( $\sim 20''$ ), suggesting again a difficulty of such interpretation that the central star is a young stellar object.

From above arguments, we are forced to conclude that the narrow-component cloud is a small dark cloulet. However, because the presence of a ring structure and spurs seen in figure 1 indicates a physical relation between the central star and the surrounding cloud, the narrow component must be a part of the object, which is physically associated with the central star, even though they may not be the gas ejecta from the central star or hypothetical companion. In order to check the possibility of YSO further, it might be nice to observe CO and  $\text{CO}_2$  ice absorption bands at  $4.2\text{--}4.7 \mu\text{m}$  (as a revelation of molecular clouds: Gibb et al. 2000) and crystalline  $\text{H}_2\text{O}$  at  $44/62 \mu\text{m}$  (as a revelation of post-AGB outflows; Maldoni et al. 2003) for the future work .

It is probably the best to perform mm-wave interferometric observations with high spatial resolution in order to clarify the physical relation between the narrow and broad components. Preliminary results of interferometric mapping of the CO  $J=1-0/2-1$  emissions with Nobeyama and Berkeley-Illinois-Maryland Arrays gave that the broad component was partially resolved in  $\sim 3''$  beam, but the narrow component is extended to about more than  $10''$  in

size. These results are consistent with the 45-m mapping observations (Paper I), and they fit well to the present interpretation that the broad component is the expanding envelope of the AGB/post-AGB object which is surrounded with a cool cloud at the distance of  $2.5 \text{ kpc}$ .

#### 4. Conclusion

We have detected a variety of molecular lines of O-, C- and N-bearing molecules toward IRAS 19312+1950, a bipolar nebula. The line profiles consist of narrow and broad components of the widths of  $\sim 4$  and  $\sim 30 \text{ km s}^{-1}$ , respectively. From the parabolic line shape, the broad component is inferred to originate from the circumstellar envelope of this object. The LVG calculations suggest the mass loss rate of about  $2.6 \times 10^{-4} M_{\odot} \text{ yr}^{-1}$  for this object. However, the origin of the narrow component is still a puzzle; from the low temperature and variety of molecules detected, it is suggested to be a dark cloulet with a mass of about  $20 M_{\odot}$ . If it were a trapped material by a hypothetical companion, the  $\text{H}_2/\text{CO}$  mass ratio must be a factor of 10 less than the value normally assumed. If this is really a dark cloud with a mass more than  $20 M_{\odot}$ , how the AGB/post-AGB star can accommodate a cloud more massive than the star mass ? Furthermore, if this is a low-mass young stellar object with SiO masers more than a few kpc away, it is hard to explain the apparent size of the bright nebulosity and luminosity of the central star.

It is hard to provide a reasonable interpretation for this object except considering somewhat exotic, previously unknown, star model as a hypergiant (Jura et al. 2001), or possibly an AGB/post-AGB object with the huge orbiting gas reservoir in which the  $\text{H}_2/\text{CO}$  ratio is small compared with a normal ratio. Another extreme is a low-mass young stellar object with SiO masers with yet undeveloped CO outflow but shining the surrounding dust of the size of  $30''$ . Neither of them could be acceptable, except with excuse if they were extreme objects.

The authors thank Dr. M. Tamura, and K. Murakawa for providing them with the SIRIUS image of IRAS 19312+1950. They also thank Dr. T. Umemoto for useful suggestions, and students (H. Fukushi, and Y. Tamura) for help of observations.

#### References

- Amano, T. 1988, *ApJ*, 329, L121
- Bergman, P. , Kerschbaum, F., & Olofsson, H. 2000, *A&A*, 353, 257
- Blake, G. A., van Dishoek, E. F., Jansen, D. J., Groesbeck, T. D., & Mundy, L. G. 1994, *ApJ*, 428, 680
- Blöcker, T. 1995, *A&A*, 297, 727
- Bujarrabal, V., Fuente, A., & Omont, A. 1994, *ApJ*, 421, L47
- Castets, A., Duvert, G., Dutrey, A., Bally, J., Langer, W. D., & Wilson, R. W. 1990, *A&A*, 234, 469
- Charnley, S. B., Tielens, A. G. G. M., & Kress, M. E. 1995, *MNRAS* 274, L53
- Charnley, S. B., & Latter, W. B. 1997, *MNRAS*, 287, 53



- Chin, Y.-N., Henkel, C., Whiteoak, J. B., Langer, N., & Churchwell, E. B. 1996, *A&A*, 305, 960
- Claude, S. M. X., Avery, L. W., & Matthews, H. E. 2000, *ApJ*, 545, 379
- Deguchi, S. 1977, *PASJ*, 29, 669
- Deguchi, S., & Goldsmith, P.F. 1985, *Nature* 317, 336
- Deguchi, S., Izumiura, H., Kaifu, N., Mao, X., Nguyen-Q-Rieu, & Ukita, N. 1990, *ApJ*, 351, 522
- Deguchi, S., Fujii, T., Matsumoto, S., Nakashima, J., & Wood, P.R. 2000, *PASJ* 53, 293
- Dickens, J. E., Irvine, W. M., Snell, R. L., Bergin, E. A., Schloerb, F. P., Pratap, P., & Miralles, M. P. 2000, *ApJ*, 542, 870
- Ehrenfreund, P., & Charnley, S. B. 2000, *ARA&A*, 38, 427
- Engels, D., Schmid-Burgk, J., & Walmsley, C. M. 1986, *A&A* 167, 129
- Fresneau, A., Vaughan, A. E., & Argyle, R. W. 2003, *AJ*, 125, 1519
- Friberg, P., Hjalmarson, A., Madden, S. C., & Irvine, W. M. 1988, *A&A*, 195, 281
- Fukasaku, S., Hirahara, Y., Masuda, A., Kawaguchi, K., Ishikawa, S., Kaifu, N., Irvine, W. M. 1994, *ApJ*, 437, 410
- Fuller, G. A., Myers, P. C., Welch, W. J., Goldsmith, P. F., Langer, W. D., Campbell, B. G., Guilloteau, S., & Wilson, R. W. 1991, *ApJ*, 376, 135
- Gibb, E. L., Whittet, D. C. B., Schutte, W. A., Boogert, A. C. A., Chiar, J. E., Ehrenfreund, P., Gerakines, P. A., Keane, J. V., Tielens, A. G. G. M., van Dishoeck, E. F., & Kerkhof, O. 2000, *ApJ*, 536, 347
- Gredel, R., van Dishoeck, E. F., & Black, J. H. 1994, *A&A*, 285, 300
- Griv, E., Gedalin, M., & Yuan, C. 1997, *A&A*, 328, 531
- Guilloteau, S., Lucas, R., Omont, A., & Nguyen-Q-Rieu 1986, *A&A*, 165, L1
- Glassgold, A. E. 1996, *ARA&A*, 34, 241
- Guelin, M., Forestini, M., Valiron, P., Ziurys, L. M., Anderson, M. A., Cernicharo, J., & Kahane, C. 1995, *A&A*, 297, 183
- Hodapp, K. 1994, *ApJS*, 94, 615
- Jiang, B. W., Szczerba, R., & Deguchi, S. 2000, *A&A*, 362, 273
- Jura, M., Kahane, C., & Omont, A. 1988, *A&A* 201, 80
- Jura, M., & Kahane, C. 1999, *ApJ*, 521, 302
- Jura, M., Velusamy, T., & Werner, M. W. 2001, *ApJ*, 556, 408
- Kahane, C., Cernicharo, J., Gomez-Gonzalez, J., & Guelin, M. 1992, *A&A*, 256, 235
- Kahane, C., Barnbaum, C., Uchida, K., Balm, S. P., & Jura, M. 1998, *ApJ*, 500, 446
- Kawaguchi, K., Kagi, E., Hirano, T., Takano, S., & Saito, S. 1993, *ApJ*, 406, L39
- Kerschbaum, F., & Olofsson, H. 1999, *A&AS*, 138, 299
- Langer, W. D., & Penzais, A. 1993, *ApJ*, 408, 539
- Latter, W. B., & Chanley, S. B. 1996, *ApJ*, 465, L81
- Le Bertre, T., Deguchi, S., & Nakada, Y. 1990 *A&A* 235, L5
- Lloyd-Evans, J. 1990, *MN*, 243, 336
- Lovas, F. J. 1992, *J. Phys. Chem. Ref. Data*, 21, 181
- Lucas, R., & Liszt, H. 1998, *A&A*, 337, 246
- MacLeod, G. C., van der Walt, D. J., North, A., Gaylard, M. J., Galt, J. A., & Moriarty-Schieven, G. H. 1998, *AJ*, 116, 2936
- Maldoni, M. M., Egan, M. P., Smith, R. G., Robinson, G., & Wright, C. M. 2003, *MNRAS*, 345, 912
- Momose, M., Ohashi, N., Kawabe, R., Nakano, T., & Hayashi, M. 1998, *ApJ*, 504, 314
- Morris, M., & Alcock, C. 1977, *ApJ*, 218, 687
- Morris, M., Guilloteau, S., Lucas, R., & Omont, A. 1987, *ApJ*, 321, 888
- Morris, M., Lucas, R., & Omont, A. 1985, *A&A* 142, 107
- Nakada, Y., Izumiura, H., Onaka, T., Hashimoto, O., Ukita, N., Deguchi, S., & Tanabe, T. 1987, *ApJ*, 323, L77
- Nakashima, J., & Deguchi, S. 2000, *PASJ* 52, L43
- Nakashima, J. & Deguchi, S. 2004, *ApJL*, 610, L41
- Nakashima, J. Deguchi, S., & Kuno, N. 2004, *PASJ*, 56, 193 (Paper I)
- Nejad, L. A. M., & Wagenblast, R. 1999, *A&A*, 350, 204
- Olofsson, H., Lindqvist, M., Nyman, L.-Å., & Winnberg, A. 1998, *A&A*, 29, 1059
- Omont, A., Lucas, R., Morris, M., & Guilloteau, S. 1993, *A&A*, 267, 490
- Park, Y.-S., & Hong, S. S. 1995, *A&A*, 300, 890
- Redman, M. P., Viti, S., Cau, P., Williams, D. A. 2003, *MNRAS*, 345, 1291
- Reipurth, B., & Bally, J. 2001, *ARA&A*, 39, 403
- Sahai, R., & Wannier, P. G. 1992, *ApJ*, 394, 320
- Savage, C., Apponi, A. J., Ziurys, L. M., & Wyckoff, S. 2002, *ApJ*, 578, 211
- Schöer, F. L., & Olofsson, H. 2000, *A&A*, 359, 586
- Swade, D. A., 1989, *ApJ*, 345, 828
- Szymczak, M., Hrynek, G., & Kus, A. J. 2000, *A&AS*, 143, 269
- Takaba, H., Iwate, T., Miyaji, T., & Deguchi, S. 2001, *PASJ*, 53, 517
- Tiemann, E. 1974, *J. Phys. Chem. Ref. Data*, 3, 259
- Townes, C. H., & Shawlow, A. L. 1975, "Microwave Spectroscopy" (Dover; New York)
- Turner, B. E. 1998, *ApJ*, 501, 731
- Wilson, T. L., & Matteucci, F. 1992, *A&ARv*, 4, 1
- Woods, P. M., Schöier, F. L., Nyman, L.-Å., & Olofsson, H. 2003, *A&A*, 402, 617
- Willems, F. J., & de Jong, T. 1986, *ApJ* 309, L39

This figure "fig1.jpg" is available in "jpg" format from:

<http://arxiv.org/ps/astro-ph/0410252v1>



This figure "fig2.jpg" is available in "jpg" format from:

<http://arxiv.org/ps/astro-ph/0410252v1>

This figure "fig3.jpg" is available in "jpg" format from:

<http://arxiv.org/ps/astro-ph/0410252v1>

This figure "fig4.jpg" is available in "jpg" format from:

<http://arxiv.org/ps/astro-ph/0410252v1>

This figure "fig5.jpg" is available in "jpg" format from:

<http://arxiv.org/ps/astro-ph/0410252v1>

This figure "fig6.jpg" is available in "jpg" format from:

<http://arxiv.org/ps/astro-ph/0410252v1>

This figure "fig7.jpg" is available in "jpg" format from:

<http://arxiv.org/ps/astro-ph/0410252v1>